ANTIOXIDANTS & REDOX SIGNALING
Volume 20, Number 14, 2014

DOI: 10.1089/ars.2013.5240

ORIGINAL RESEARCH COMMUNICATION

Role of Unfolded Protein Response Dysregulation in Oxidative Injury of Retinal Pigment Epithelial Cells

Chen Chen,[1,2] Marisol Cano,[3] Joshua J. Wang,[1,2,4] Jingming Li,[2] Chuangxin Huang,[1,5] Qiang Yu,[5] Terence P. Herbert,[6] James T. Handa,[3] and Sarah X. Zhang[1,2,4,7]

Abstract

Aims: Age-related macular degeneration (AMD), a major cause of legal blindness in the elderly, is associated with genetic and environmental risk factors, such as cigarette smoking. Recent evidence shows that cigarette smoke (CS) that contains high levels of potent oxidants preferably targets retinal pigment epithelium (RPE) leading to oxidative damage and apoptosis; however, the mechanisms are poorly understood. The present study aimed to investigate the role of endoplasmic reticulum (ER) stress and the unfolded protein response (UPR) in CS-related RPE apoptosis. ***Results:*** ER stress and proapoptotic gene C/EBP homologous protein (*CHOP*) were induced in the RPE/choroid complex from mice exposed to CS for 2 weeks and in human RPE cells treated with hydroquinone, a potent oxidant found at high concentrations in CS. Suppressing ER stress or inhibiting CHOP activation by pharmacological chaperones or genetic approaches attenuated hydroquinone-induced RPE cell apoptosis. In contrast to enhanced CHOP activation, protein level of active X-box binding protein 1 (XBP1), a major regulator of the adaptive UPR, was reduced in hydroquinone-treated cells. Conditional knockout of *XBP1* gene in the RPE resulted in caspase-12 activation, increased CHOP expression, and decreased antiapoptotic gene Bcl-2. Furthermore, *XBP1*-deficient RPE cells are more sensitive to oxidative damage induced by hydroquinone or NaIO3, a CS-unrelated chemical oxidant. Conversely, overexpressing XBP1 protected RPE cells and attenuated oxidative stress-induced RPE apoptosis. ***Innovation and Conclusion:*** These findings provide strong evidence suggesting an important role of ER stress and the UPR in CS-related oxidative injury of RPE cells. Thus, the modulation of the UPR signaling may provide a promising target for the treatment of AMD. *Antioxid. Redox Signal.* 20, 2091–2106.

Introduction

Age-related macular degeneration (AMD) is a leading cause of blindness among the elderly in Western countries, and its prevalence is expected to increase significantly in the next decade owing to the rapidly growing aging population (1, 4). Clinically, AMD is classified into dry (nonneovascular) and wet (neovascular) AMD. Dry AMD affects 85%–90% of people with AMD, and a small number of dry AMD can transform into wet AMD characterized by abnormal growth of new blood vessels from the choroid into the macula. The advanced form of dry AMD, also called geographic atrophy, and wet AMD is responsible for most severe vision loss caused by the disease. A major pathological hallmark of dry AMD is age-dependent degenerative damage of the retinal pigment epithelium (RPE), a monolayer of hexagonal epithelial cells located adjacent to and physically interacted with retinal photoreceptors (45). Normal function of RPE cells is required for maintaining photoreceptor cell survival, neuroretinal hemostasis, and visual function. In advanced dry AMD, RPE atrophy is often accompanied by photoreceptor degeneration (45). Despite many recent

[1]Department of Ophthalmology/Ross Eye Institute, University at Buffalo, The State University of New York, Buffalo, New York.
[2]Department of Medicine and Endocrinology, University of Oklahoma Health Sciences Center, Oklahoma City, Oklahoma.
[3]Wilmer Eye Institute, Johns Hopkins School of Medicine, Baltimore, Maryland.
[4]SUNY Eye Institute, The State University of New York, Buffalo, New York.
[5]State Key Laboratory of Ophthalmology, Zhongshan Ophthalmic Center, Sun Yat-sen University, Guangzhou, China.
[6]Department of Cell Physiology and Pharmacology, University of Leicester, Leicester, United Kingdom.
[7]Department of Biochemistry, University at Buffalo, The State University of New York, Buffalo, New York.

Innovation

Cigarette smoking is a major environmental risk factor for age-related macular degeneration (AMD). Cigarette smoke (CS) preferably damages retinal pigment epithelium (RPE) cells through oxidative stress resulting in RPE apoptosis; however, the mechanisms are poorly understood. In this study, we provided the first evidence that endoplasmic reticulum (ER) stress and the activation of the proapoptotic unfolded protein response (UPR) are implicated in RPE apoptosis induced by chemical oxidants, CS, hydroquinone, and NaIO3. In addition, hydroquinone suppresses X-box binding protein 1 (XBP1)-mediated adaptive UPR, which is essential for RPE cell survival during oxidative stress. These findings strongly argue that ER stress, and more importantly, dysregulated UPR signaling, contributes to CS-related and oxidative injury of RPE cells in relation to AMD.

advances in clinical management of wet AMD, such as photodynamic and anti-VEGF therapies, interventions that prevent or halt the progression of RPE degeneration and photoreceptor loss are currently not available.

The pathogenesis of AMD is complex involving a variety of genetic and environmental factors. Among the environmental factors, cigarette smoking was identified as the strongest and most consistent risk factor for AMD (9). Clinical studies have revealed that people who smoke are up to four times more likely than nonsmokers to develop AMD and suffer vision loss (51). Chronic exposure of C57BL/6 mice to cigarette smoke (CS) resulted in mitochondrial DNA damage, oxidative injury, and apoptosis of RPE cells (12, 53). Exposure to CS or hydroquinone, a potent pro-oxidant that presents at high concentration in cigarette tar, led to disrupted basal infolding of the RPE, sub-RPE deposits, and thickened Bruch's membrane (10, 12, 53). Hydroquinone also suppresses the RPE expression of monocyte chemoattractant protein 1 resulting in reduced recruitment of scavenging macrophages and accumulation of proinflammatory debris in the RPE (44). These findings indicate that CS and smoke-related oxidants induce RPE injury to some extent. However, these changes are not sufficient to cause severe RPE degeneration and drusen formation as seen in human AMD (10). Additional mechanisms apart from the mild oxidative injury may be implicated in the pathogenesis of RPE damage in this disease (10).

The endoplasmic reticulum (ER) is a central hub in the cell responsible for the biosynthesis and post-translational modification of secretory and membrane proteins. Conditions that lead to an imbalance between protein synthesis and protein folding disrupt the ER homeostasis resulting in ER stress (24). In response to the stress, cells have evolved an intricate set of signaling pathways named the unfolded protein response (UPR) to restore the ER homeostasis. If this process fails, ER stress will activate the apoptotic cascades triggering cell death (56). A variety of ER stress-related genes are involved in ER stress-associated apoptosis (40), such as caspase-12 and C/EBP homologous protein (CHOP). The deletion of CHOP protects cells from ER stress-induced apoptosis in various disease models (11, 39, 49). In contrast, loss of X-box binding protein 1 (XBP1), a master regulator of the adaptive UPR, exacerbates cell death (23, 47). In addition, our recent study has implied XBP1 in redox regulation and cell survival in the RPE (59). Conditional knockout of *XBP1* gene in RPE cells resulted in increased oxidative stress and apoptosis in the RPE, accompanied by mild cone photoreceptor loss and defect in retinal function (59). These findings suggest that the UPR signaling may be implicated in RPE degeneration during AMD. In this study, we investigated the role of ER stress and the UPR in RPE cell injury induced by chemical oxidants, including CS, hydroquinone, and NaIO3. Our results indicate that ER stress contributes, at least in part, to RPE apoptosis and that XBP1-mediated adaptive UPR plays an important role in protecting RPE cells from oxidative damage.

Results

CS causes differential changes in ER stress and UPR genes in mouse retina and RPE

CS is a complex chemical mixture that contains high concentrations of oxidants and free radicals and is a potent inducer of oxidative damage and apoptosis of RPE cells (3). To determine if ER stress is involved in CS-induced oxidative RPE injury and retinal degeneration, we examined the expression of major ER stress response genes in the retina and RPE/choroid complex from mice exposed to CS for 2 weeks, 2 months, and 6 months. Two weeks after the exposure to CS, the expression of *CHOP*, an ER stress-inducible proapoptotic gene, increased by fourfold in the RPE/choroid complex, which was accompanied by enhanced splicing of *XBP1* mRNA (Fig. 1). These changes indicate an induction of ER stress in the RPE. With prolonged exposure, *CHOP* expression declined to normal levels by 2 and 6 months, whereas *XBP1* splicing continued to increase at 2 months, but declined by 6 months of CS treatment. Interestingly, while the level of spliced *XBP1* mRNA was significantly higher in mice after 2 weeks and 2 months of CS exposure, the expression of *P58ipk*, a major *XBP1* target gene (25), in the RPE/choroid from the same mice was not altered. This suggests that the function/activity of *XBP1* may be suppressed in the RPE by CS. In contrast to the upregulation of *CHOP* in RPE/choroid complex, *CHOP* expression did not change in the retina at any time point of CS exposure (Fig. 1). *XBP1* splicing was increased in the retina after 2 and 6 months of CS exposure. Notably, increased spliced *XBP1* mRNA level coincided with enhanced *p58ipk* expression, suggesting that *XBP1* function in the retina is intact.

Hydroquinone induces ER stress in human RPE cells

To further confirm the presence of ER stress in CS-related oxidative injury of RPE cells, we treated a human RPE cell line, ARPE-19 cells, with hydroquinone, one of the potent oxidants in CS. Apoptotic markers, mitochondrial cytochrome *c* release and caspase 3 activation, were also measured in cells after the exposure to hydroquinone for 0–6 h to determine whether oxidative stress promoted the cells to enter apoptosis. Our results show that the expression of 78 kD glucose-regulated protein (GRP78), a major ER chaperone involved in protein folding, was increased rapidly in hydroquinone-treated cells (Fig. 2A, B). XBP1 splicing, a result of inositol-requiring enzyme 1α (IRE1α) activation, was induced as early as 1 h and lasted at least 6 h after hydroquinone exposure (Fig. 2C). In parallel, hydroquinone induced a time-dependent PKR-like ER kinase

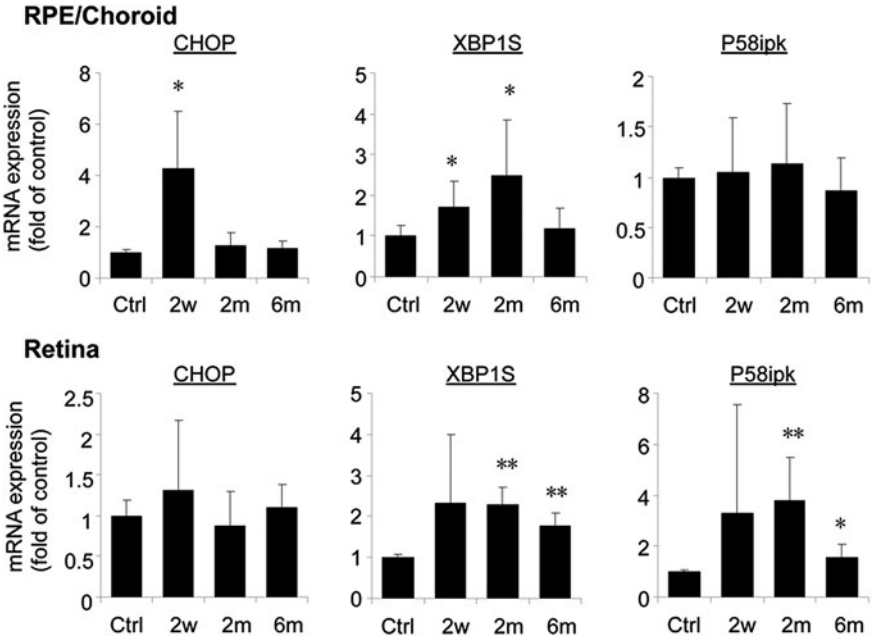

FIG. 1. Expression of ER stress response genes in the retina and RPE/choroid complex from mice exposed to CS. Eight-week-old C57/BL6 mice were exposed to cigarette smoking for 2 weeks, 2 months, and 6 months. Age-matched control mice were kept in a filtered air environment. Expression of *CHOP*, spliced *XBP1*, and *P58ipk* in the RPE/choroid complex and in the retina from CS-exposed and control mice were measured by quantitative real-time PCR. Data were expressed as mean ± SD ($n = 5$ in each group). $^{*}p < 0.05$, $^{**}p < 0.01$ *versus* controls. CHOP, C/EBP homologous protein; ER, endoplasmic reticulum; RPE, retinal pigment epithelium; XBP1, X-box binding protein 1.

(PERK) phosphorylation (Fig. 2D), accompanied by an increased phosphorylation of eukaryotic translation initiation factor 2α (eIF2α) (Fig. 2E). These changes were followed by enhanced nuclear activating transcription factor 4 (ATF4) and CHOP, downstream effectors of the PERK/eIF2α pathway (Fig. 2F). To further determine if ER stress is implicated in apoptosis, we assessed the levels of pro- and cleaved caspase-4, which is an ER resident, and a counterpart of murine caspase-12 in human, only activated by ER stress leading to caspase-3 activation and apoptosis (20). We found that caspase-4 was activated by hydroquinone in a time-dependent manner (Fig. 2G). In line with these results, the level of cleaved caspase-3 was increased, reflecting the activation of caspase-3 in hydroquinone-treated cells (Fig. 2H). As oxidative stress and mitochondrial dysfunction have been proposed to play a role in CS-induced RPE cell damage (53), we examined cytochrome *c* release from mitochondria. We observed that hydroquinone markedly increased cytochrome *c* release into the cytosol (Fig. 2I), which supports a role of mitochondria in hydroquinone-induced RPE cell apoptosis.

Inhibition of ER stress abolishes CHOP activation and alleviates hydroquinone-induced RPE cell apoptosis

To determine if ER stress is essential for hydroquinone-induced RPE cell apoptosis, two structurally distinct chemical chaperones, 4-phenyl butyric acid (PBA) (54) and tauroursodeoxycholate (TUDCA) (41, 55), were used to inhibit ER stress in ARPE-19 cells. Pretreatment with PBA or TUDCA dose dependently attenuated CHOP activation in hydroquinone-treated cells (Fig. 3A). Hydroquinone-induced nuclear translocation of CHOP was also abolished (Fig. 3B). As expected, PBA and TUDCA markedly alleviated hydroquinone-induced apoptosis and cell death (Fig. 3C–E). Furthermore, we examined whether the protective effect of PBA and TUDCA prevents mitochondrial dysfunction. We found that cytochrome *c* release was not altered by either PBA or TUDCA (Fig. 3F). These results suggest that ER stress is required for hydroquinone-induced RPE apoptosis and that inhibition of ER stress by chemical chaperones might suppress the apoptotic process downstream of cytochrome *c* release.

Inhibition of CHOP activation ameliorated hydroquinone-induced apoptosis in RPE cells

CHOP has been shown to be a major mediator of ER stress-associated apoptosis in various cell types (40, 41, 48, 55). To elucidate the role of CHOP activation in RPE cell apoptosis, we used adenoviruses expressing dominant negative PERK (Ad-PERKDN) or an N-terminal deletion mutant of growth-arrest and DNA-damage-inducible protein 34 (GADD34, Ad-GADD34ΔN), which targets protein phosphatase-1 to eIF2α causing its constitutively dephosphorylation (36). Upon PERK inhibition, eIF2α phosphorylation was attenuated in RPE cells (Fig. 4A). Similarly, overexpressing GADD34ΔN also inhibited eIF2α phosphorylation (Fig. 4B). As a consequence, CHOP activation, as indicated by nuclear levels of CHOP, induced by hydroquinone, was almost completely abolished (Fig. 4C, D). Consistently, hydroquinone-induced apoptosis was significantly inhibited in Ad-PERKDN- and Ad-GADD34ΔN-treated cells. Ad-PERKDN and Ad-GADD34ΔN alone had no effect on cell survival or morphology (Fig. 4E, F).

XBP1 protects RPE cells from hydroquinone-induced apoptosis

XBP1 is a central regulator of the adaptive UPR during ER stress. We intended to address how XBP1 is implicated in RPE cell damage induced by CS. We first examined the protein expression of spliced XBP1 in hydroquinone-treated cells. To our surprise, we found that despite increased splicing of XBP1 mRNA, the protein level of spliced XBP1 was drastically decreased in hydroquinone-treated cells (Fig. 5A). Moreover, inhibition of protein degradation by proteasome inhibitor MG132 did not reverse the reduction in spliced XBP1 protein

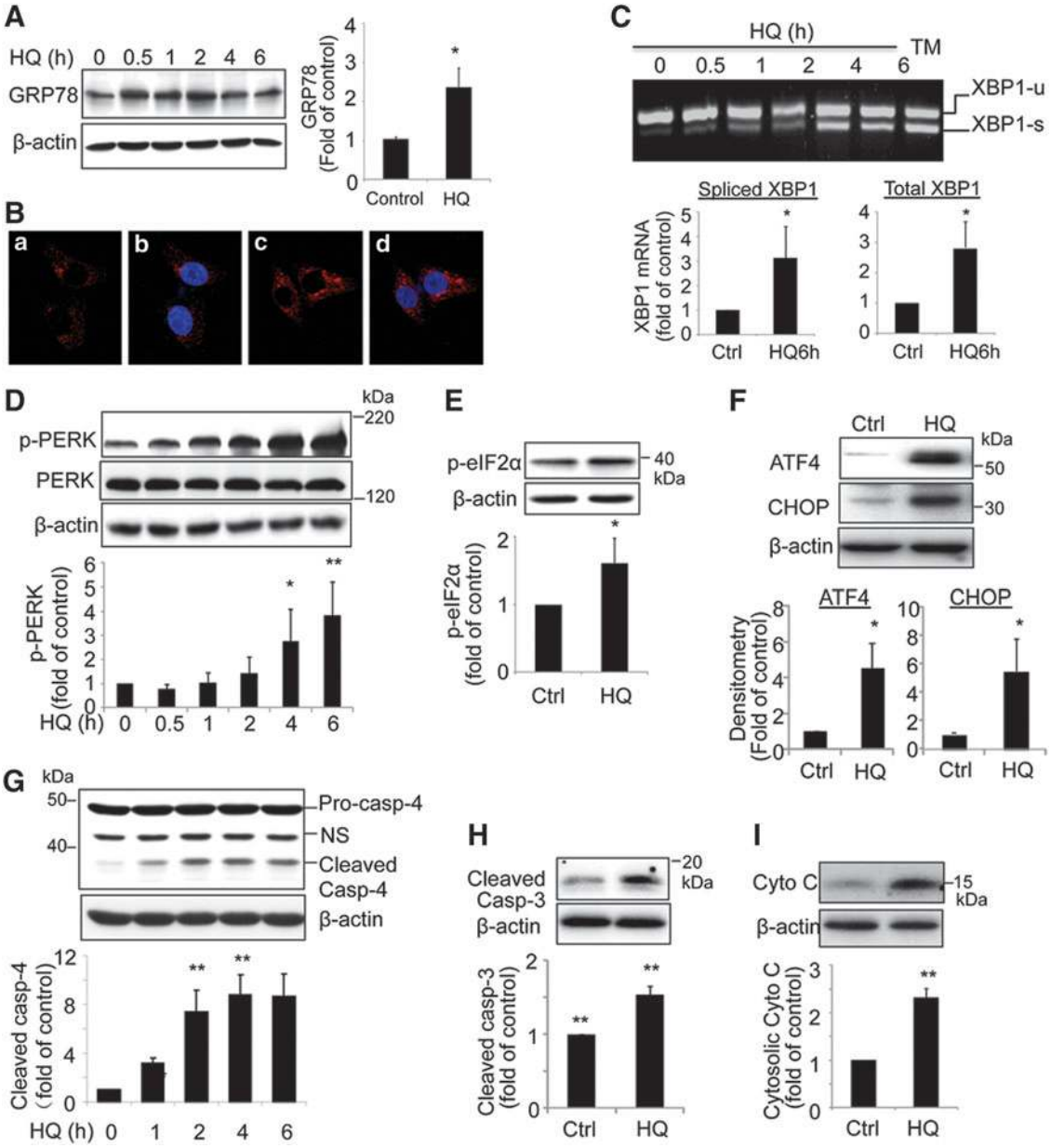

FIG. 2. HQ induces ER stress and apoptosis in human RPE cells. ARPE-19 cells were treated with HQ (100 μM) for 0–6 h. **(A)** Protein levels of GRP78 were determined by Western blot analysis. *Left panel:* representative blots. *Right panel:* densitometry results of GRP78 protein levels at 2 h after HQ treatment. **(B)** Immunocytochemistry of GRP78 (red) in cells treated with HQ for 2 h. DAPI was used to stain cell nuclei (blue). **(a, b)** control; **(c, d)** HQ for 2 h. **b** and **d** are merged images of GRP78 (red) and DAPI staining (blue). Magnification: 1000×. **(C)** *XBP1* splicing was detected by RT-PCR (*left panel*) and real-time PCR (*right panels*). Cells exposed to tunicamycin (50 ng/ml) for 6 h were used as a positive control. **(D, E)** Levels of phospho-PERK **(D)** and phospho-eIF2α **(E)** were determined by Western blot analysis. *Lower panels:* densitometry results. **(F)** Expression of ATF4 and CHOP was measured by Western blot analysis using nuclear extracts. **(G)** Levels of pro- and cleaved caspase 4 were assessed by Western blot analysis and quantified by densitometry. **(H)** Cleaved caspase 3 was determined in whole cell lysate. **(I)** Cytosolic cytochrome *c* was detected by Western blot analysis. All data were expressed as mean ± SD from three independent experiments. $*p < 0.05$, $**p < 0.01$. ATF4, activating transcription factor 4; eIF2α, eukaryotic translation initiation factor 2α; GRP78, glucose-regulated protein; HQ, hydroquinone; PERK, PKR-like ER kinase. To see this illustration in color, the reader is referred to the web version of this article at www.liebertpub.com/ars

(Fig. 5B), which suggests that the inhibition was proteasome-independent. To explore the role of XBP1 in RPE cell survival, we overexpressed spliced XBP1 by adenovirus in ARPE-19 cells. As expected, overexpressing XBP1 inhibits eIF2α phosphorylation and CHOP activation (Fig. 5C, D) and protected RPE cells from hydroquinone-induced apopotosis (Fig. 5E). Conversely, knockdown of XBP1 using siRNA resulted in apoptosis in unstimulated RPE cells and further exacerbated hydroquinone-induced cell death (Fig. 5F, G). These results suggest that XBP1 is a crucial survival factor in RPE cells.

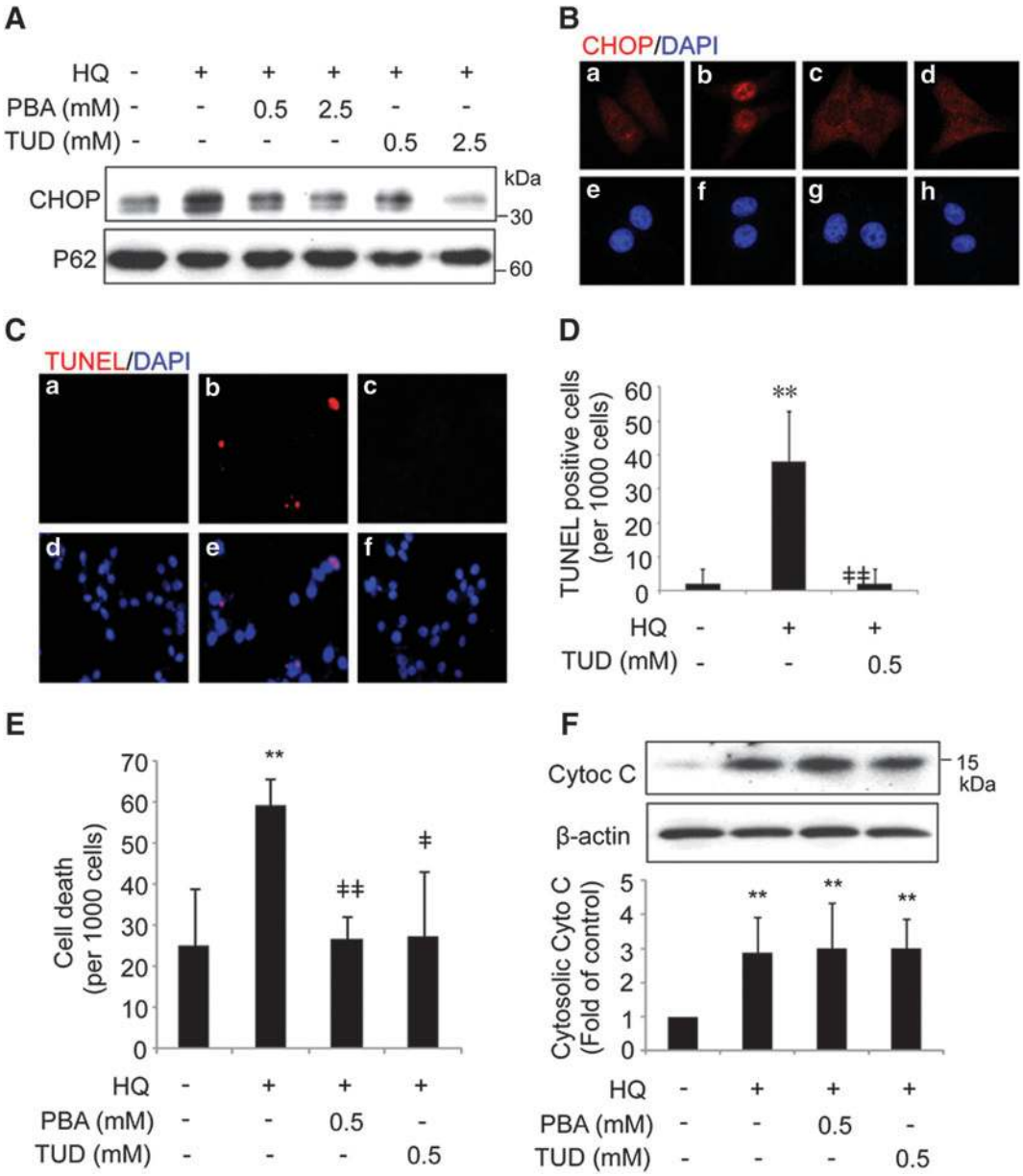

FIG. 3. Inhibition of ER stress and CHOP activation protects RPE cells against HQ-induced apoptosis without altering cytochrome *c* release. ARPE-19 cells were pretreated with chemical chaperone PBA or TUDCA for 12 h, followed by HQ (100 μM) treatment for 6 or 24 h. CHOP expression and cytosolic cytochrome C were measured at 6 h **(A, B, F)**, whereas apoptosis and cell death were examined at 24 h **(C–E)** after the treatment **(A)**. Nuclear expression of CHOP was determined by Western blot analysis. **(B)** Immunocytochemistry demonstrates increased expression of CHOP (red) and nuclear translocation after HQ treatment, which was abolished by pretreatment with PBA and TUDCA. Blue: nuclear staining with DAPI. Magnification: 400×. **(a, e)** control; **(b, f)** HQ; **(c, g)** HQ+PBA; **(d, h)** HQ+TUDCA. **(C)** Cell apoptosis was determined by TUNEL assay. Red: TUNEL staining of apoptotic cells; Blue: nuclear staining with DAPI. Magnification: 400×. **(a, d)** control; **(b, e)** HQ; **(c, f)** HQ+TUDCA; **(D)** Quantification of TUNEL-positive cells. **(E)** Quantification of cell death using the trypan blue method. **(F)** Level of cytosolic cytochrome *c* was detected by Western blot analysis. Data were expressed as mean±SD from three independent experiments. $^{**}p < 0.01$ *versus* control, $^{‡}p < 0.05$, $^{‡‡}p < 0.01$ *versus* HQ. PBA, 4-phenyl butyric acid; TUDCA, tauroursodeoxycholate; TUNEL, terminal deoxynucleotidyl transferase dUTP nick end labeling. To see this illustration in color, the reader is referred to the web version of this article at www.liebertpub.com/ars

Loss of XBP1 sensitizes RPE cells to hydroquinone-induced apoptosis through regulation of CHOP and Bcl-2

To further confirm the role of endogenous XBP1 in the RPE, primary RPE cells were isolated from RPE-*XBP1* knockout ($XBP1^{-/-}$) and littermate *XBP1* flox/flox ($XBP1^{+/+}$) mice. A representative image of mouse RPE cells is shown in Fig. 6A. Downregulation of XBP1 is indicated by a decreased XBP1 protein in the presence of MG132 (Fig. 6B). When compared to $XBP1^{+/+}$ cells, $XBP1^{-/-}$ cells exhibited increased caspase-12 activation and expressed lower levels of antiapoptotic gene

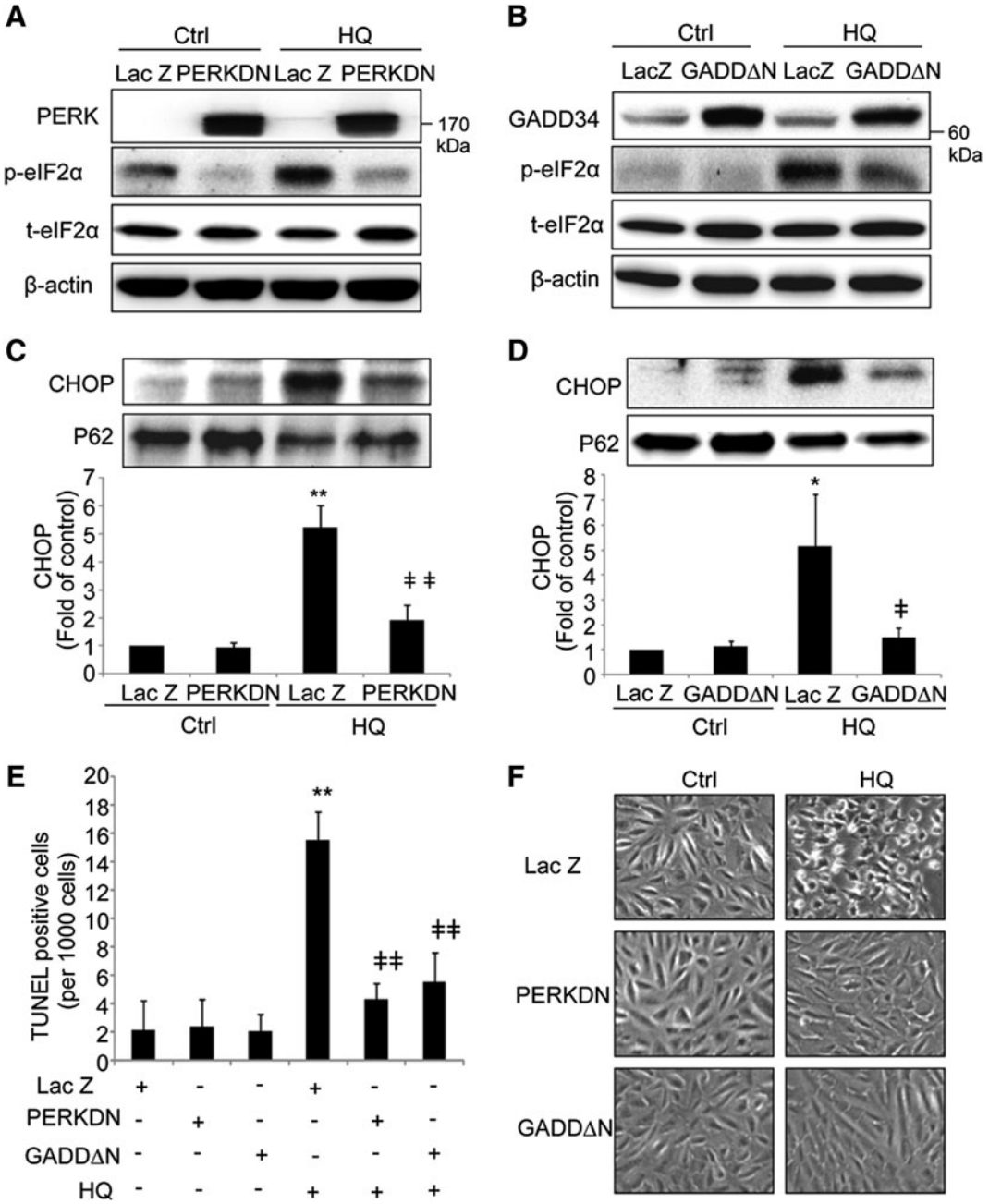

FIG. 4. Inhibition of PERK and eIF2α phosphorylation abolishes HQ-induced CHOP activation and apoptosis of RPE cells. ARPE-19 cells were transfected with adenovirus expressing dominant negative PERK (PERKDN) or GADD34ΔN, followed by HQ treatment for 6 or 24 h. Adenovirus expressing LacZ was used as control. **(A, B)** Levels of phospho- and total eIF2α were determined by Western blot analysis. **(C, D)** Nuclear CHOP levels were measured by Western blot analysis and quantified by densitometry. **(E)** Apoptosis of RPE cells was examined by TUNEL assay after HQ treatment for 24 h. **(F)** Representative phase-contrast images after HQ 24 h treatment in RPE cells. Magnification: 100×. $n = 3$. $^{*}p < 0.05$, $^{**}p < 0.01$ *versus* control, $^{\ddagger}p < 0.05$, $^{\ddagger\ddagger}p < 0.01$ *versus* HQ.

Bcl-2 (Fig. 6C, D). After hydroquinone treatment, CHOP was significantly induced in $XBP1^{-/-}$ cells at a much higher level than in $XBP1^{+/+}$ cells (Fig. 6E, F). Terminal deoxynucleotidyl transferase dUTP nick end labeling (TUNEL) staining showed an increased number of apoptotic cells in $XBP1^{-/-}$ RPE cells under both untreated and hydroquinone-treated conditions when compared to $XBP1^{+/+}$ cells (Fig. 6G, H). These results suggest that the loss of XBP1 sensitizes RPE cells to hydroquinone-induced apoptosis. To determine if XBP1 regulates anti- and proapoptotic genes, we examined mRNA expression of *CHOP* and antiapoptotic gene *Bcl-2* in RPE explants from *XBP1* knockout mice. We found that Bcl-2 level was significantly lower in $XBP1^{-/-}$ mouse RPE than $XBP1^{+/+}$ RPE, and the difference was more remarkable after hydroquinone incubation (Fig. 7A). In the untreated condition, CHOP mRNA level in $XBP1^{-/-}$ mouse RPE was double that

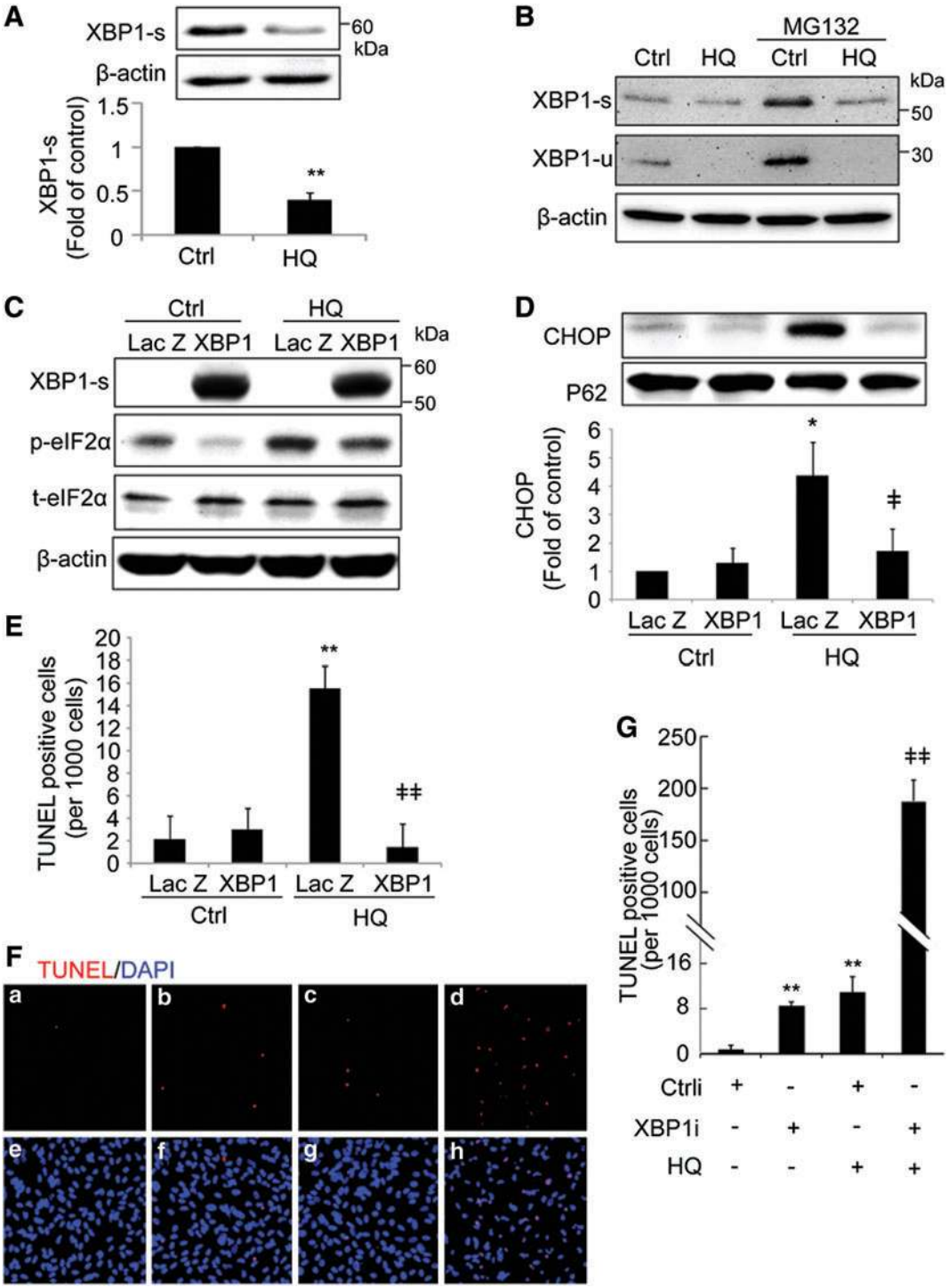

FIG. 5. XBP1 protects RPE cells from HQ-induced apoptosis. (A) Protein level of spliced XBP1 in ARPE-19 cells after HQ treatment for 6 h. *Lower panel:* densitometry of Western blots. **(B)** Protein level of spliced and unspliced XBP1 after HQ treatment with or without proteasome inhibitor MG132. **(C–E)** ARPE-19 cells were transfected with adenovirus expressing spliced XBP1 followed by HQ treatment. Adenovirus expressing LacZ was used as control. Level of phospho- and total eIF2α **(C)** in the whole cell lysate and expression of CHOP **(D)** in the nucleus were detected by Western blot analysis. Apoptosis of RPE cells was examined by TUNEL assay **(E)** after HQ treatment for 24 h. **(F, G)** ARPE-19 cells were transfected with siRNA against XBP1 or scrambled siRNA as control. Transfected cells were exposed to HQ for 24 h. Apoptosis was determined by TUNEL assay. Representative pictures of TUNEL staining were shown in **(F)**. Red: TUNEL staining of apoptotic cells; blue: nuclear staining with DAPI. Magnification: 100×. **(a, e)** Ctrli; **(b, f)** XBP1i; **(c, g)** Ctrli + HQ; **(d, h)** XBP1i + HQ. Quantification of TUNEL-positive cells was shown in **(G)**. $^{*}p < 0.05$, $^{**}p < 0.01$ *versus* control, $^{‡}p < 0.05$, $^{‡‡}p < 0.01$ *versus* HQ. To see this illustration in color, the reader is referred to the web version of this article at www.liebertpub.com/ars

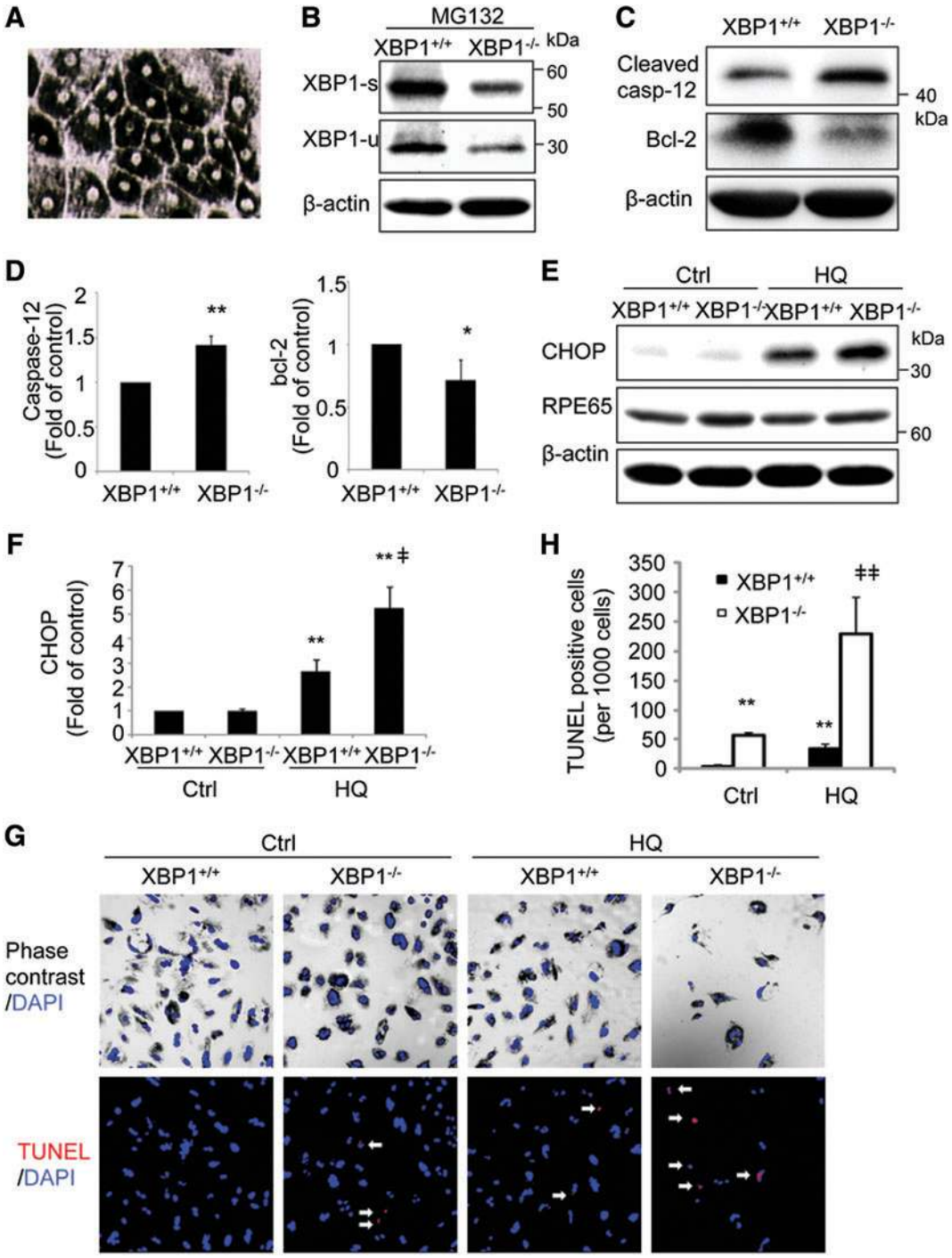

FIG. 6. Loss of XBP1 augments HQ-induced CHOP expression and exacerbates apoptosis in primary RPE cells from RPE-specific XBP1 KO mice. (A) Representative phase contrast image of isolated mouse RPE cells. Magnification: 100×. **(B)** Expression of spliced and unspliced XBP1 in RPE cells isolated from wild-type ($XBP1^{+/+}$) and RPE-specific XBP1 KO ($XBP1^{-/-}$) mice after treatment with proteasome inhibitor MG132. **(C, D)** Expression of cleaved caspase-12 and Bcl-2 in XBP1-deficient mouse RPE cells. Results were quantified by densitometry **(D)**. **(E, F)** CHOP expression was determined by Western blot analysis in RPE cells treated with HQ (50 μM) for 8 h. **(G)** Apoptosis was examined by TUNEL assay in RPE cells after HQ (50 μM) treatment for 24 h. *Upper panels:* phase-contrast images merged with DAPI staining of nuclei (blue). *Lower panels:* TUNEL staining (red) merged with DAPI (blue). Magnification: 100×. *Arrow:* TUNEL-positive cells. **(H)** Quantification of TUNEL-positive cells. $^{*}p < 0.05$, $^{**}p < 0.01$ *versus* untreated $XBP1^{+/+}$ cells, $^{\ddagger}p < 0.05$, $^{\ddagger\ddagger}p < 0.01$ *versus* $XBP1^{+/+}$ cells treated with HQ. To see this illustration in color, the reader is referred to the web version of this article at www.liebertpub.com/ars

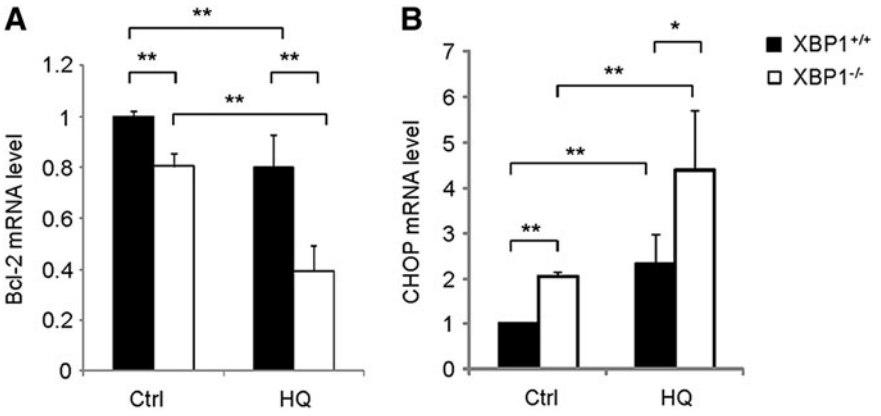

FIG. 7. Decreased *Bcl-2* and increased *CHOP* expression in *XBP1*-deficient mouse RPE explants. Isolated single layer of mouse RPE was incubated in growth medium with or without HQ (50 μM) for 6 h. Total RNA was extracted immediately after incubation. mRNA expression of *Bcl-2* **(A)** and *CHOP* **(B)** was measured by real-time RT-PCR. Results were expressed as mean ± SD. For Bcl-2, $n = 6$. For CHOP, $XBP1^{+/+}$: $n = 4$, $XBP1^{-/-}$: $n = 6$. *$p < 0.05$, **$p < 0.01$.

observed in $XBP1^{+/+}$ mouse RPE, which was further increased after hydroquinone incubation (Fig. 7B). These results together indicate that normal function of XBP1 is essential for protecting RPE cells from oxidative stress-induced damage and apoptosis.

NaIO3 induces RPE cell apoptosis through ER stress

To determine whether ER stress is involved in RPE cell apoptosis induced by other oxidants, we treated ARPE-19 cells with a potent reactive oxidant, NaIO3, and measured the ER stress and apoptosis after exposure for up to 24 h. Six hours after NaIO3 treatment, ER stress markers, including PERK and eIF2α phosphorylation, XBP1 splicing, and CHOP expression, were significantly upregulated (Fig. 8A–C). Notably, the nuclear level of spliced XBP1 was increased in NaIO3-treated cells. Apoptosis was induced after 24 h of NaIO3 treatment and was largely prevented by pretreatment of cells with PBA or TUDCA (Fig. 8D, E). These results suggest that NaIO3 induces RPE cell apoptosis, at least partially, through ER stress.

XBP1 knockout exacerbates NaIO3-induced RPE damage and photoreceptor degeneration in mice

To further evaluate the role of endogenous XBP1 in RPE cells *in vivo*, RPE degeneration was induced with systemic injection of NaIO3 in wild-type and *XBP1* knockout mice. NaIO3 selectively targets the RPE resulting in an acute injury of RPE cells followed by a secondary apoptosis and degeneration of photoreceptors (22, 30). In contrast, the CS model only demonstrates relatively mild changes of the RPE, including oxidative damage, ultrastructural abnormalities, and apoptosis, and these changes take at least 6 months to develop (12, 53). Thus, we chose the NaIO3 model to investigate the role of XBP1 in oxidative damage of the RPE. Consistent with previous reports (22, 30), in wild-type ($XBP1+/+$) mice, RPE cell apoptosis was observed by 6 h after injection, peaked at 12 h, and declined by 24 h after tail vein injection of NaIO3 (Fig. 9A). Photoreceptor apoptosis was not observed until 24 h after injection, peaked at 3 days, and diminished by 5 days (Fig. 9A). Compared with $XBP1^{+/+}$ mice, $XBP1^{-/-}$ mice had significantly increased RPE apoptosis at 6 h after injection, which was accompanied by a higher number of apoptotic photoreceptor cells (Fig. 9B). We next examined retinal histology in NaIO3-treated mice. In wild-type mice, NaIO3 induced a time-dependent RPE atrophy and degenerative change of choriocapillaries, accompanied by loss of photoreceptor cells (reduction in outer nuclear layer [ONL] thickness), disorganization of the inner segment/outer segment (IS/OS) junction, and inflammatory cell infiltration (Fig. 9C). When compared to $XBP1^{+/+}$ mice, $XBP1^{-/-}$ mice exhibited more severe damage in the RPE and photoreceptors, as evidenced by much thinner RPE layer and ONL, disruption of the IS/OS junction, and more inflammatory cells (Fig. 9D, E). These results suggest that the loss of XBP1 potentiates oxidative damage of the RPE.

Discussion

It is well established that cigarette smoking is an important risk factor for AMD and is highly associated with RPE injury (33) and progressive loss of RPE in advanced dry AMD (8). CS contains high concentrations of free radicals and a large number of pro-oxidants, which have been shown to induce oxidative damage in various organs and tissues (2, 3, 50). In animals, CS induces mitochondrial DNA damage and apoptosis to RPE cells (12, 53); however, the molecular mechanisms underlying CS-related and oxidative RPE damage are poorly understood. In the present study, we investigated the implication of ER stress and the UPR in RPE apoptosis induced by different chemical oxidants and our results suggest that ER stress and dysregulated UPR induced by CS and oxidative stress in general may play a role in RPE cell death.

CHOP, also known as growth-arrest and DNA damage-inducible gene 153 (GADD153), is an ER stress-associated proapoptotic gene and belongs to the C/EBP family. It is expressed at very low levels under physiological conditions but upregulated robustly in response to perturbations that induces severe or persistent ER stress. We observed CHOP induction, mediated primarily by the PERK-eIF2α-ATF4 pathway, in RPE cells treated with hydroquinone or NaIO3. As a transcription factor, CHOP has been shown to suppress antiapoptotic genes such as Bcl-2 and upregulates proapoptotic genes such as Bax (32), PUMA (13), and tribbles-related protein 3 (TRB3) (5), contributing to ER stress-related apoptosis. In hydroquinone-treated RPE cells, suppressing PERK-eIF2α activation by various approaches reduces levels of CHOP and protects RPE cells from apoptosis, suggesting a role of ER stress and CHOP in RPE apoptosis. In addition, enhancing CHOP activity could deplete cellular glutathione and exaggerate ROS production leading to disturbance in cellular redox status (32). The impact of CHOP on oxidative

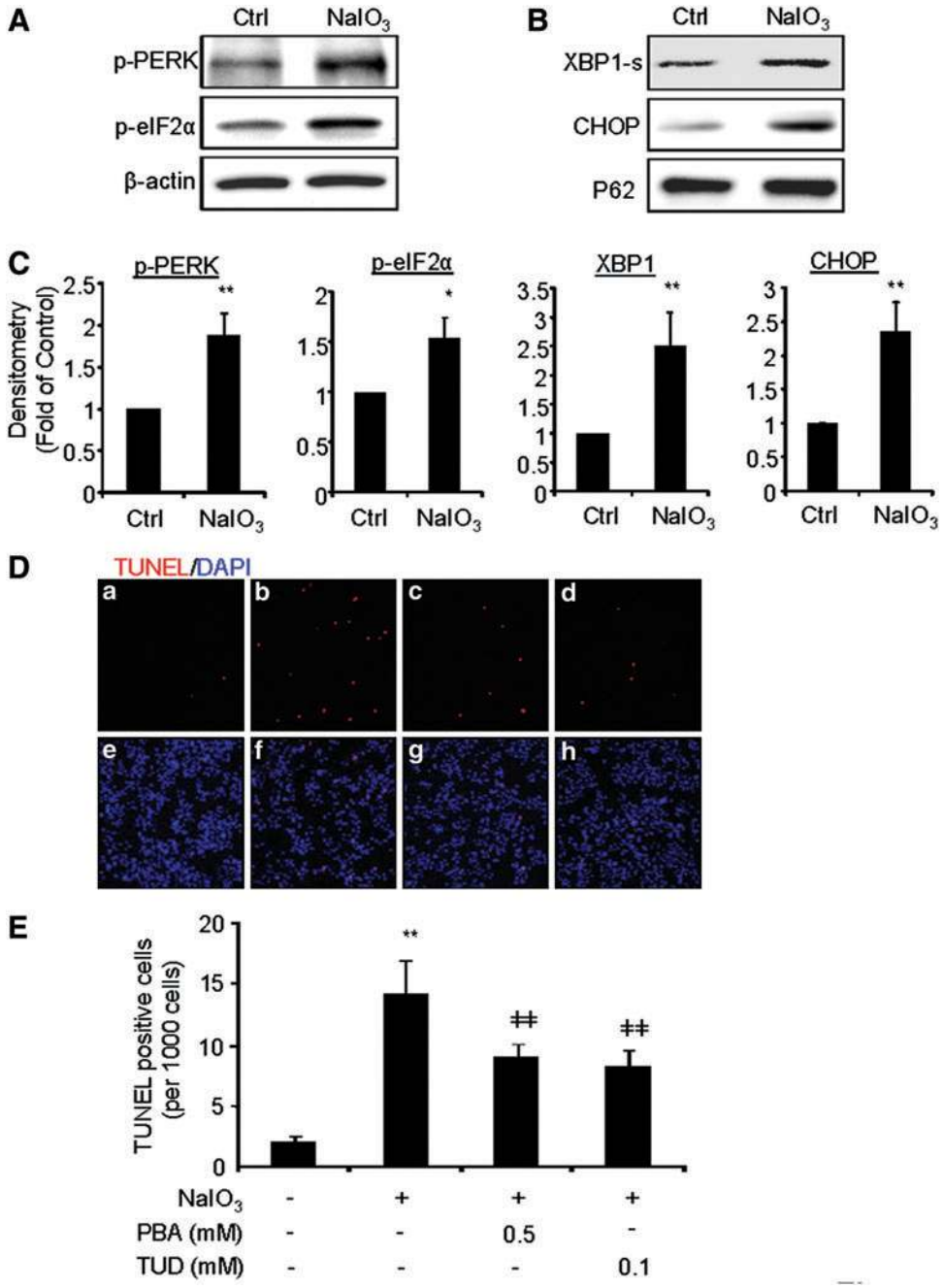

FIG. 8. NaIO3 induces ER stress and apoptosis in ARPE-19 cells. (A–C) ARPE-19 cells were treated with NaIO3 (200 ng/ml) for 6 h, and ER stress markers (p-PERK, p-eIF2α, spliced XBP1, and CHOP) were determined by Western blot analysis and quantified by densitometry. Data were expressed as mean ± SD (n = 3 independent experiments). **(D, E)** ARPE-19 cells were treated with NaIO3 (200 ng/ml) for 24 h with or without PBA or TUDCA pretreatment. Cell apoptosis was determined by TUNEL assay. **(a, e)** control; **(b, f)** HQ treatment; **(c, g)** PBA 0.5 m*M* pretreated; **(d, h)** TUDCA 0.1 m*M* pretreated. Magnification: 100×. **(E)** Quantification of TUNEL-positive cells. *$p < 0.05$, **$p < 0.01$, *versus* control. ‡‡$p < 0.01$ *versus* NaIO3. To see this illustration in color, the reader is referred to the web version of this article at www.liebertpub.com/ars

stress in RPE cells is yet to be investigated. Interestingly, although increased CHOP expression is often seen in conditions with intense or prolonged ER stress, we observed a temporal induction of CHOP in mouse RPE after short-term exposure to CS. While the unexpected decline in CHOP expression after 2 and 6 months of CS exposure may reflect the complex *in vivo* situation, we suspect that these changes could be related to a negative feedback mechanism that tightly regulates the CHOP expression/activity. Indeed, studies by Ohoka *et al.* (38) and Jousse *et al.* (21) suggest that TRB3, one of the CHOP target genes that promote apoptosis, also acts as a regulator of CHOP reducing its expression and suppressing its transactivation. Whether CHOP is regulated by such a feedback mechanism involving TRB3 and/or other regulatory molecules in RPE cells warrants future investigation.

In contrast to increasing CHOP expression, hydroquinone reduces XBP1 protein level in RPE cells, despite inducing its mRNA splicing. This result corroborates our *in vivo* finding which suggests that XBP1 activity may be blunted in RPE/choroid complex from mice exposed to CS. Interestingly, reduction in XBP1 protein was not observed in RPE cells treated with NaIO3, another potent but CS-unrelated oxidant, which indicates a differential regulation of UPR by distinct oxidants. Furthermore, inhibiting proteosomal activity did not rescue the reduction in XBP1 protein by hydroquinone. This suggests a potential effect of hydroquinone and CS on XBP1 protein synthesis. In a previous study, Carbonnelle and associates (6) reported that hydroquinone inhibited IL-1α and IL-1β protein synthesis in human monocytes. Acrolein, another major component of CS, also reduces protein synthesis in

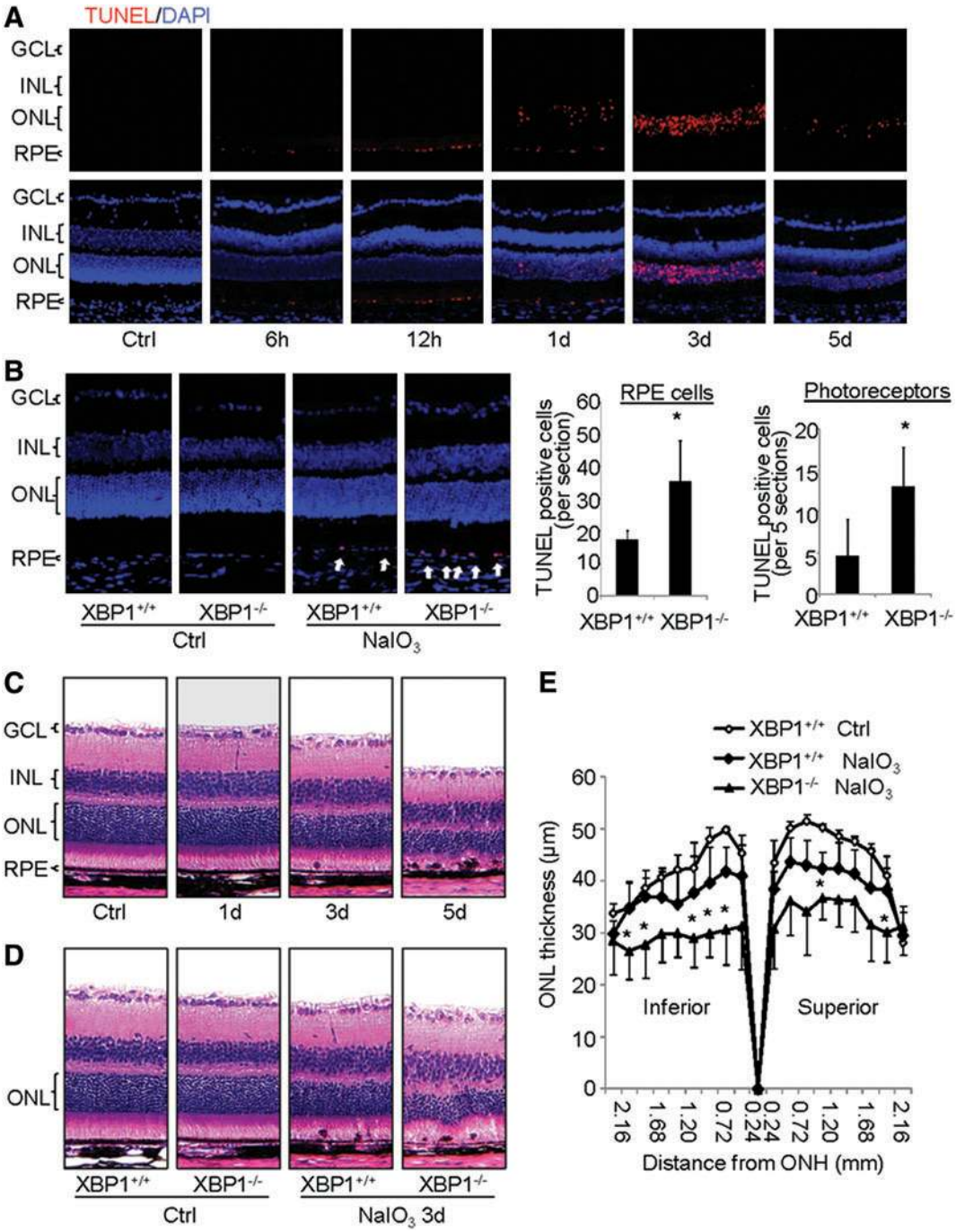

FIG. 9. Knockout of *XBP1* in the RPE exaggerates NaIO3-induced RPE damage and photoreceptor degeneration in mice. Wild-type and RPE-specific *XBP1* KO mice were injected NaIO3 (30 mg/kg body weight) through lateral tail vein and sacrificed at various time points. **(A)** TUNEL staining of eye sections from wild-type mice at different time points after injection. Red: TUNEL. Blue: DAPI. **(B)** TUNEL staining of eye sections from untreated or NaIO3-treated wild-type and *XBP1* KO mice at 6 h after injection. *Left panel:* representative images. Magnification: 200×. Red: TUNEL. Blue: DAPI. *Arrow:* TUNEL-positive RPE cells. *Right panel:* quantification of TUNEL-positive RPE cells per section (average of five sections per mouse eye) and photoreceptor cells (expressed as sum of five sections). Mean ± SD, $XBP1^{+/+}$: $n = 5$, $XBP1^{-/-}$: $n = 7$. $^*p < 0.05$. **(C)**. Histology of eye sections from wild-type mice at different time points after injection. **(D)** Histology of eye sections from wild-type and *XBP1* KO mice 3 days after NaIO3 injection. **(E)** Quantification of ONL thickness in wild-type and *XBP1* KO mice 3 days after NaIO3 injection. Mean ± SD, $XBP1^{+/+}$ no treatment: $n = 4$, $XBP1^{+/+}$ NaIO3: $n = 5$, $XBP1^{-/-}$ NaIO3: $n = 6$. $^*p < 0.05$. GCL, ganglion cell layer; IPL, inner plexiform layer; INL, inner nuclear layer; OPL, outer plexiform layer; ONL, outer nuclear layer; IS, inner segment; OS, outer segment. To see this illustration in color, the reader is referred to the web version of this article at www.liebertpub.com/ars

pulmonary artery endothelial cells (42). In line with these studies, a recent clinical research shows that the basal rate of skeletal protein synthesis was markedly reduced in middle- and older-aged heavy smokers compared with age-matched individuals who had never smoked (43). Since RPE cells synthesize and secrete many growth factors and enzymes, which are important for visual activity and neural retinal homeostasis, the potential effect of CS-related oxidants on RPE protein synthesis worth further investigation (44, 57).

Our data emphasize a role of XBP1 in protecting RPE cells against oxidative damage imposed by hydroquinone or NaIO3. XBP1 is a basic leucine zipper transcription factor activated by IRE1 during ER stress (16). Active XBP1 induces a large set of UPR genes, predominantly ER chaperones such as p58ipk (16), and has been reported to exert anti-apoptotic function in cancer cells (17) and neurons (7). However, sustained expression of XBP1 inhibits beta-cell function and induces apoptosis in aortic endothelial cells (58). In the present study, we investigated the role of XBP1 in oxidative injury of RPE cells. We found that overexpressing spliced XBP1 protected RPE cells from hydroquinone-induced apoptosis, whereas the deletion of *XBP1* gene led to decreased Bcl-2 and exacerbated CHOP expression in the RPE. Moreover, mice deficient of *XBP1* in RPE cells developed more profound RPE apoptosis and photoreceptor loss in the NaIO3 model. These observations, together with previous finding reported by Lin and colleagues that persistent ER stress suppresses IRE1 and ATF6 activity resulting in apoptosis (28), provide strong evidence that integrity of the adaptive UPR is important for RPE cell survival.

Although we have shown a role of ER stress in RPE apoptosis, our findings do not rule out the role of mitochondrial dysfunction and oxidative stress in CS-associated tissue injury, which has been shown by many elegant studies (12, 53). Similar to mitochondria, the ER is extremely sensitive to oxidative stress and is a major target of endogenous ROS generated during aging (37). In aged mouse liver, several major ER chaperones such as protein disulfide isomerase and GRP78 were oxidatively modified, resulting in the decline in protein folding activities and ER stress (37). It is possible that the induction of ER stress by CS, hydroquinone, and NaIO3 is mediated by a common mechanism, namely oxidative stress. Future studies are needed to test this hypothesis. Another interesting finding from our study is that chemical chaperones protect RPE cells without altering cytosolic cytochrome *c* level. This may suggest that these chaperones suppress the apoptotic process downstream of cytochrome *c* release. Indeed, PBA has been shown to upregulate heat shock protein 70 (HSP70), which acts downstream of cytochrome C and suppresses caspase-3 activation (19, 26). In addition, we observed that the loss of XBP1 increased the activation of caspase-12, a proapoptotic enzyme specifically activated by ER stress but not by membrane- or mitochondrial-targeted apoptotic signals (35). We also observed a time-dependent activation of caspase-4 by hydroquinone in ARPE-19 cells. Caspase-4 is the counterpart of murine caspase-12 and functions as an ER-specific caspase in humans (20). Activated caspase-12 (caspase 4 in humans) cleaves pro-caspase-9 into active caspase-9, which in turn activates caspase-3, leading to apoptosis (34). Caspase-12 can also be activated by its downstream executioner caspase-7 to form an amplification loop in the apoptotic cascades (46). Mice lacking caspase-12 are resistant to ER stress-induced apoptosis (35). Notably, in caspase-12-mediated apoptosis, cytochrome *c* is not released from mitochondria, which suggests that cytochrome *c* is not involved in the caspase-12-dependent apoptosis (34). Future studies that investigate the role of caspase-12 in RPE apoptosis may help in developing new approaches that target apoptotic cascades involving both the ER and mitochondria and protect the RPE in AMD.

Materials and Methods

Animals

All animal procedures were conducted according to the ARVO Statement for the Use of Animals in Ophthalmic and Vision Research and approved by the Institutional Animal Care and Use Committees at the University of Oklahoma Health Sciences Center or by the Institutional Research Board at the Johns Hopkins Medical Institutions. C57BL/6 (wild-type) mice were purchased from the Jackson Laboratory. RPE-specific *XBP1* knockout mice were generated by crossing *XBP1* flox/flox mice, which contains two loxP sites in the exon 2 of *XBP1* gene, with RPE-specific *cre* transgenic mice, which express Cre recombinase in the RPE (59). Littermates that were Cre recombinase negative were used as controls in all experiments. All mice were maintained on a 12-h light–dark cycle and were allowed free access to standard rodent chow and water *ad libitum*.

Exposure to CS

An equal number of male and female C57BL/6 mice were used for the experiments. At 8 weeks of age, mice were placed into a smoking chamber for 2.5 h/day, 5 days/week for 2 weeks, 2 months, and 6 months. This chamber contains a smoking machine (Model TE-10; Teague Enterprises) that burns five cigarettes (2R4F reference cigarettes, 2.45 mg nicotine/cigarette; Tobacco Research Institute, University of Kentucky) at a time, taking 2 s duration puffs at a flow rate of 1.05 L/min, to provide a standard puff of 35 cm^3, providing a total of eight puffs per minute. The machine is adjusted to produce side stream (89%) and mainstream smoke (11%). The chamber atmosphere is monitored to maintain total suspended particulate at 250 mg/m^3. Control mice were kept in a filtered air environment. After CS exposure, mice were sacrificed, eyes were harvested, and retinas and RPE/choroids were dissected for RNA extraction.

Cell culture

Human RPE (ARPE-19) cells were purchased from the American Type Culture Collection (ATCC) and maintained in the DMEM/F12 medium containing 10% fetal bovine serum and 1% antibiotic/antimycotic. For all experiments, undifferentiated cells were grown to 90% confluence and quiescent overnight with the serum-free DMEM/F12 medium before treatment.

Transduction of adenoviruses and transfection of siRNA in ARPE-19 cells

ARPE-19 cells at 50%–60% confluence were transduced with adenoviruses expressing PERK-DN (18), GADD34ΔN (18), or spliced XBP1 (27). Adenovirus expressing LacZ or

GFP was used as control. After 24 h transduction, cells were quiescent overnight with the serum-free DMEM/F12 medium before treatment. ARPE-19 cells at 40%–50% confluence were transfected with XBP1 siRNA or control siRNA (Santa Cruz Biotechnology) using Lipofectamine 2000 (Invitrogen) following the manufacturer's instruction (27). Cells were quiescent overnight with the serum-free DMEM/F12 medium before treatment.

Immunocytochemistry

Immediately after treatment, cells were fixed with 4% paraformaldehyde for 20 min at room temperature and then permeabilized with 0.1% Triton X-100 for 10 min. After blocking with 1% BSA for 1 h, cells were incubated with anti-GRP78 (1:100; Abacm) or anti-CHOP (1:100; Santa Cruz Biotechnology) at 4°C overnight. After incubation with Cy3-conjugated secondary antibody (1:500; Jackson Immunoresearch Laboratories), fluorescence was observed and pictures were taken under a FluoView FV500 confocal laser scanning microscope (Olympus).

Primary RPE cell culture

Primary mouse RPE cells were isolated as previously described (15) with minor modification. Briefly, 14-day-old mice were sacrificed by cervical dislocation, and eyeballs enucleated. Ten to 16 eyes were pooled, washed in 5 ml DMEM/F12 medium and then digested with 2% (wt/vol) dispase (GIBCO; #17105-041) in DMEM/F12 at 37°C for 1 h. After digestion, anterior segments of the eyeballs were removed, and neural retinas were discarded. Single RPE sheets were peeled off the eyecups and centrifuged in growth medium at 1500 rpm for 3 min. The pellet was digested with 0.05% trypsin and the resulting single cells were seeded in 12-well plates and grown for 7–10 days until confluent. To insure sufficient Cre recombinase expression, RPE cells from RPE-*XBP1* knockout mice were transduced with adenovirus expressing Cre recombinase, and the cells from *XBP1* flox/flox mice were transfected with adenovirus expressing GFP as control.

RPE explants and hydroquinone incubation

Mouse RPE sheets were isolated as described above. RPE sheets from one mouse (two eyeballs) were pooled and incubated with the growth medium in the presence or absence of hydroquinone (50 μM) in a 12-well plate at 37°C for 6 h. Immediately after incubation, total RNA was extracted and used for quantitative real-time PCR.

NaIO3 injection, TUNEL assay, and histology study in mice

NaIO3 was purchased from Sigma, dissolved in PBS at 5 mg/ml, and filtered before use. Mice were injected with NaIO3 (30 mg/kg body weight) through the tail vein and sacrificed from 6 h to 5 days after injection. Eyeballs were enucleated and prepared for cryosectioning or paraffin sectioning as described previously (27). Cryosections were cut at 7 μm thickness through the optic nerve and used for TUNEL assay. For each eyeball, five sections with 50 μm intervals were stained with TUNEL, and the average TUNEL-positive RPE cell number per section was used for statistical analysis. Paraffin sections were cut along the vertical meridian through the optic nerve at 5 μm thickness and stained with hematoxylin and eosin. The thickness of ONL was measured under a light microscope using SPOT Advanced imaging software (SPOT Imaging Solutions). Measurements were taken every 240 μm from the optic nerve head to the peripheral retina in both the superior and inferior portions of the retina as described previously (31).

Western blot analysis

For extraction of total cellular protein, cells were lysed in RIPA buffer with protease inhibitor cocktail, PMSF and sodium orthovanadate (Santa Cruz Biotechnology). Nuclear protein was extracted using a nuclear extract kit (Active Motif; #40010). For detection of cytochrome *c* release, the cytosolic portion was prepared as described previously (29). Protein concentration was quantified using the BCA kit (Pierce Biotechnology, Inc.). Twenty-five micrograms of protein was resolved by SDS-PAGE gel and electrotransferred to nitrocellular membranes. After blocking, membranes were blotted overnight at 4°C with following primary antibodies: anti-p-PERK (1:1000), anti-ATF4 (CREB2, 1:1000), anti-CHOP (GADD153, 1:1000), anti-GADD34 (1:1000), anti-XBP1 (1:500; Santa Cruz Biotechnology), anti-p-eIF2a (1:1000), anti-cleaved caspase-3 (1:500), anti-PERK (1:1000), anti-cleaved caspase-12 (1:500; Cell Signaling Technology), anti-caspase-4 (1:1000; Medical & Biological Laboratories Co., Ltd.), anti-Bcl-2 (1:1000; BD Biosciences), anti-GRP78 (1:1000; Abcam), and anti-eIF2α (1:1000; Novus Biologicals). Anticytochrome *c* (1:1000) and anti-RPE65 (1:1000) antibodies were kindly gifts from Dr. Luke Szweda (Oklahoma Medical Research Foundation) and Dr. Jian-xing Ma (University of Oklahoma Health Sciences Center), respectively. After incubation with HRP-conjugated secondary antibodies, membranes were developed with chemiluminescence substrate (Thermo Fisher Scientific; #34076) using Vision Works LS image acquisition and analysis software (UVP). Membranes were reblotted with anti-β-actin (1:5000; Abcam) or anti-Nucleoporin-P62 (1:1000; BD Biosciences) for normalization. The bands were semi-quantified by densitometry using the same software.

RT-PCR and quantitative real-time PCR

Total RNA were extracted from ARPE-19 cells and mouse tissues using an E.Z.N.A. total RNA kit I (Omega bio-tek) or an RNeasy Mini Kit (Qiagen) following the manufacturers' instructions. cDNA was synthesized using a Maxima First Strand cDNA synthesis kit (Fermentas) or a High Capacity cDNA Reverse Transcription kit (Applied Biosystems). To investigate XBP1 splicing, RT-PCR was performed using the cDNA template and PCR Master Mix (Fermentas; #K1081) as described previously, and PCR products were resolved on a 2.5% agarose/1× TAE gel (28). Quantitative real-time PCR was performed on a StepOnePlus Real-Time PCR System (Applied Biosystems) or Bio-Rad Real-Time PCR System (Bio-Rad Laboratories) according to the manufacturers' recommendations using the following primers: human total *XBP1*: forward 5′-CCATGGATTCTGGCGGTATTGACT-3′, reverse 5′-CCACATTAGCTTGGCTCTCTGTCT-3′; human spliced *XBP1*: forward, 5′-CCGCAGCAGGTGCAGG-3′, reverse 5′-GAGTCAATACCGCCAGAATCCA-3′ (14); mouse spliced *XBP1*: forward 5′-ACACGCTTGGGAATGGACAC-3′, reverse 5′ CCATGGGAAGATGTTCTGGG-3′; mouse *Bcl-2*: forward

5′-CCTGGCATCTTCTCCTTC-3′, reverse 5′-GCTGACTGGA CATCTCTG-3′; mouse *CHOP*: forward 5′-GTCCCTAGCTT GGCTGACAGA-3′, reverse 5′-TGGAGACGCAGGGCTTTG-3′ (52); mouse *P58ipk*: forward 5′TCCTGGTGGACCTGCAG TACG-3′, reverse 5′-CTGCGAGTAATTTCTTCCCC 3′. Data were analyzed by the comparative threshold cycle method using 18s ribosomal RNA or β-actin as an internal control.

TUNEL assay in cultured RPE cells

Apoptosis was detected using the In Situ Cell Death Detection TMR red kit (TUNEL Assay; Roche Diagnostics Corp.) according to manufacturer's protocol both for cells and for cryosections. Briefly, for cells, coverslips were fixed with 4%PFA for 1 h, followed by permeabilization for 2 min on ice in 0.1% citrate buffer containing 0.1% Triton X-100. Then, coverslips were incubated at 37°C in TUNEL reaction mix containing nucleotides and terminal deoxynucleotidyl transferase (TdT). Incubation without TdT enzyme was conducted as a negative control. After three washes of PBS, coverslips were mounted to a slide with a mounting medium for fluorescence with DAPI (Vector Laboratories; #H-1200). For tissue, cryosections were rinsed in PBS to remove the OCT compound and then subjected to the same procedures as for cells.

Statistical analysis

The quantitative data were expressed as mean ± SD. Statistical analyses were performed using unpaired Student's *t*-test when comparing two groups and one-way analysis of variance with Bonferroni's multiple comparison test for three groups or more. Statistical differences were considered significant at a *p*-value of less than 0.05.

Acknowledgments

We thank Drs. Laurie Glimcher and Ann-Hwee Lee (Harvard University, Boston, MA) for *XBP1*flox/flox mice; Dr. Luke Szweda (Oklahoma Medical Research Foundation) for anticytochrome *c* antibody; Dr. Jian-xing Ma for anti-RPE65 antibody; Louisa J. Williams and Linda S. Boone (Dean A. McGee Eye Institute, Oklahoma City, OK) for their help in histology; and Diabetes COBRE Histology Core (OUHSC, Oklahoma City, OK) for image acquisition. This work was supported by the National Institutes of Health grants EY019949, Research Grant M2010088 from the American Health Assistance Foundation, Research Award 7-11-BS-182 from the American Diabetes Association, Research Grant HR10-060 from the Oklahoma Center for the Advancement of Science and Technology, Dr. William Talley Research Award from Harold Hamm Diabetes Center, and Unrestricted Grants from Research to Prevent Blindness to the Department of Ophthalmology of University at Buffalo (S.X.Z); EY14005, EY019004, Thome Foundation Grant, RPB Senior Scientist Award, and the Robert Bond Welch Professorship (J.T.H.).

Author Disclosure Statement

No competing financial interests exist.

References

1. Augood CA, Vingerling JR, de Jong PT, Chakravarthy U, Seland J, Soubrane G, Tomazzoli L, Topouzis F, Bentham G, Rahu M, *et al.* Prevalence of age-related maculopathy in older Europeans: the European Eye Study (EUREYE). *Arch Ophthalmol* 124: 529–535, 2006.
2. Barreiro E, Peinado VI, Galdiz JB, Ferrer E, Marin-Corral J, Sanchez F, Gea J, and Barbera JA. Cigarette smoke-induced oxidative stress: a role in chronic obstructive pulmonary disease skeletal muscle dysfunction. *Am J Respir Crit Care Med* 182: 477–488, 2010.
3. Bertram KM, Baglole CJ, Phipps RP, and Libby RT. Molecular regulation of cigarette smoke induced-oxidative stress in human retinal pigment epithelial cells: implications for age-related macular degeneration. *Am J Physiol Cell Physiol* 297: C1200–C1210, 2009.
4. Bressler NM. Age-related macular degeneration is the leading cause of blindness. *JAMA* 291: 1900–1901, 2004.
5. Bromati CR, Lellis-Santos C, Yamanaka TS, Nogueira TCA, Leonelli M, Caperuto LC, Gorjão R, Leite AR, Anhê GF, and Bordin S. UPR induces transient burst of apoptosis in islets of early lactating rats through reduced AKT phosphorylation via ATF4/CHOP stimulation of TRB3 expression. *Am J Physiol Regul Integr Comp Physiol* 300: R92–R100, 2010.
6. Carbonnelle P, Lison D, Leroy JY, and Lauwerys R. Effect of the benzene metabolite, hydroquinone, on interleukin-1 secretion by human monocytes in vitro. *Toxicol Appl Pharmacol* 132: 220–226, 1995.
7. Casas-Tinto S, Zhang Y, Sanchez-Garcia J, Gomez-Velazquez M, Rincon-Limas DE, and Fernandez-Funez P. The ER stress factor XBP1s prevents amyloid-beta neurotoxicity. *Hum Mol Genet* 20: 2144–2160, 2011.
8. Clemons TE, Milton RC, Klein R, Seddon JM, and Ferris FL. Risk Factors for the incidence of advanced age-related macular degeneration in the age-related eye disease study (AREDS): AREDS report no. 19. *Ophthalmology* 112: 533–539.e531, 2005.
9. de Jong PTVM. Age-related macular degeneration. *N Engl J Med* 355: 1474–1485, 2006.
10. Espinosa-Heidmann DG, Suner IJ, Catanuto P, Hernandez EP, Marin-Castano ME, and Cousins SW. Cigarette smoke–related oxidants and the development of sub-RPE deposits in an experimental animal model of dry AMD. *Invest Ophthalmol Vis Sci* 47: 729–737, 2006.
11. Fu HY, Okada K, Liao Y, Tsukamoto O, Isomura T, Asai M, Sawada T, Okuda K, Asano Y, Sanada S, *et al.* Ablation of C/EBP homologous protein attenuates endoplasmic reticulum-mediated apoptosis and cardiac dysfunction induced by pressure overload. *Circulation* 122: 361–369, 2010.
12. Fujihara M, Nagai N, Sussan TE, Biswal S, and Handa JT. Chronic cigarette smoke causes oxidative damage and apoptosis to retinal pigmented epithelial cells in mice. *PLoS One* 3: e3119, 2008.
13. Galehdar Z, Swan P, Fuerth B, Callaghan SM, Park DS, and Cregan SP. Neuronal apoptosis induced by endoplasmic reticulum stress is regulated by ATF4-CHOP-mediated induction of the Bcl-2 homology 3-only member PUMA. *J Neurosci* 30: 16938–16948, 2010.
14. Gargalovic PS, Gharavi NM, Clark MJ, Pagnon J, Yang WP, He A, Truong A, Baruch-Oren T, Berliner JA, Kirchgessner TG, *et al.* The unfolded protein response is an important regulator of inflammatory genes in endothelial cells. *Arterioscler Thromb Vasc Biol* 26: 2490–2496, 2006.
15. Gibbs D, Kitamoto J, and Williams DS. Abnormal phagocytosis by retinal pigmented epithelium that lacks myosin VIIa, the Usher syndrome 1B protein. *Proc Natl Acad Sci U S A* 100: 6481–6486, 2003.

16. Glimcher LH. XBP1: the last two decades. *Ann Rheum Dis* 69 Suppl 1: i67–i71, 2010.
17. Gomez BP, Riggins RB, Shajahan AN, Klimach U, Wang A, Crawford AC, Zhu Y, Zwart A, Wang M, and Clarke R. Human X-box binding protein-1 confers both estrogen independence and antiestrogen resistance in breast cancer cell lines. *FASEB J* 21: 4013–4027, 2007.
18. Gomez E, Powell ML, Bevington A, and Herbert TP. A decrease in cellular energy status stimulates PERK-dependent eIF2Î ± phosphorylation and regulates protein synthesis in pancreatic Î²-cells. *Biochem J* 410: 485–493, 2008.
19. Gong B, Zhang L-Y, Lam DS-C, Pang C-P, and Yam GH-F. Sodium 4-phenylbutyrate ameliorates the effects of cataract-causing mutant gammaD-crystallin in cultured cells. *Mol Vis* 16: 997–1003, 2010.
20. Hitomi J, Katayama T, Eguchi Y, Kudo T, Taniguchi M, Koyama Y, Manabe T, Yamagishi S, Bando Y, Imaizumi K, *et al.* Involvement of caspase-4 in endoplasmic reticulum stress-induced apoptosis and A*ß*-induced cell death. *J Cell Biol* 165: 347–356, 2004.
21. Jousse C, Deval C, Maurin A-C, Parry L, Chérasse Y, Chaveroux C, Lefloch R, Lenormand P, Bruhat A, and Fafournoux P. TRB3 inhibits the transcriptional activation of stress-regulated genes by a negative feedback on the ATF4 pathway. *J Biol Chem* 282: 15851–15861, 2007.
22. Kiuchi K, Yoshizawa K, Shikata N, Moriguchi K, and Tsubura A. Morphologic characteristics of retinal degeneration induced by sodium iodate in mice. *Curr Eye Res* 25: 373–379, 2002.
23. Kurata M, Yamazaki Y, Kanno Y, Ishibashi S, Takahara T, Kitagawa M, and Nakamura T. Anti-apoptotic function of Xbp1 as an IL-3 signaling molecule in hematopoietic cells. *Cell Death Dis* 2: e118, 2011.
24. Lai E, Teodoro T, and Volchuk A. Endoplasmic reticulum stress: signaling the unfolded protein response. *Physiology (Bethesda)* 22: 193–201, 2007.
25. Lee A, Iwakoshi N, and Glimcher L. XBP-1 regulates a subset of endoplasmic reticulum resident chaperone genes in the unfolded protein response. *Mol Cell Biol* 23: 7448–7459, 2003.
26. Li C-Y, Lee J-S, Ko Y-G, Kim J-I, and Seo J-S. Heat shock protein 70 inhibits apoptosis downstream of cytochrome c release and upstream of caspase-3 activation. *J Biol Chem* 275: 25665–25671, 2000.
27. Li J, Wang JJ, and Zhang SX. Preconditioning with endoplasmic reticulum stress mitigates retinal endothelial inflammation via activation of X-box binding protein 1. *J Biol Chem* 286: 4912–4921, 2011.
28. Lin JH, Li H, Yasumura D, Cohen HR, Zhang C, Panning B, Shokat KM, Lavail MM, and Walter P. IRE1 signaling affects cell fate during the unfolded protein response. *Science* 318: 944–949, 2007.
29. Lundberg KC and Szweda LI. Initiation of mitochondrial-mediated apoptosis during cardiac reperfusion. *Arch Biochem Biophys* 432: 50–57, 2004.
30. Machalinska A, Lubinski W, Klos P, Kawa M, Baumert B, Penkala K, Grzegrzolka R, Karczewicz D, Wiszniewska B, and Machalinski B. Sodium iodate selectively injuries the posterior pole of the retina in a dose-dependent manner: morphological and electrophysiological study. *Neurochem Res* 35: 1819–1827, 2010.
31. Mandal MN, Patlolla JM, Zheng L, Agbaga MP, Tran JT, Wicker L, Kasus-Jacobi A, Elliott MH, Rao CV, and Anderson RE. Curcumin protects retinal cells from light-and oxidant stress-induced cell death. *Free Radic Biol Med* 46: 672–679, 2009.
32. McCullough KD, Martindale JL, Klotz LO, Aw TY, and Holbrook NJ. Gadd153 sensitizes cells to endoplasmic reticulum stress by down-regulating Bcl2 and perturbing the cellular redox state. *Mol Cell Biol* 21: 1249–1259, 2001.
33. Mitchell P, Wang JJ, Smith W, and Leeder SR. Smoking and the 5-year incidence of age-related maculopathy: the Blue Mountains Eye Study. *Arch Ophthalmol* 120: 1357–1363, 2002.
34. Morishima N, Nakanishi K, Takenouchi H, Shibata T, and Yasuhiko Y. An endoplasmic reticulum stress-specific caspase cascade in apoptosis. Cytochrome c-independent activation of caspase-9 by caspase-12. *J Biol Chem* 277: 34287–34294, 2002.
35. Nakagawa T, Zhu H, Morishima N, Li E, Xu J, Yankner BA, and Yuan J. Caspase-12 mediates endoplasmic-reticulum-specific apoptosis and cytotoxicity by amyloid-beta. *Nature* 403: 98–103, 2000.
36. Novoa I, Zhang Y, Zeng H, Jungreis R, Harding HP, and Ron D. Stress-induced gene expression requires programmed recovery from translational repression. *EMBO J* 22: 1180–1187, 2003.
37. Nuss JE, Choksi KB, DeFord JH, and Papaconstantinou J. Decreased enzyme activities of chaperones PDI and BiP in aged mouse livers. *Biochem Biophys Res Commun* 365: 355–361, 2008.
38. Ohoka N, Yoshii S, Hattori T, Onozaki K, and Hayashi H. TRB3, a novel ER stress-inducible gene, is induced via ATF4-CHOP pathway and is involved in cell death. *EMBO J* 24: 1243–1255, 2005.
39. Oyadomari S, Koizumi A, Takeda K, Gotoh T, Akira S, Araki E, and Mori M. Targeted disruption of the Chop gene delays endoplasmic reticulum stress-mediated diabetes. *J Clin Invest* 109: 525–532, 2002.
40. Oyadomari S and Mori M. Roles of CHOP/GADD153 in endoplasmic reticulum stress. *Cell Death Differ* 11: 381–389, 2004.
41. Ozcan U, Yilmaz E, Ozcan L, Furuhashi M, Vaillancourt E, Smith RO, Gorgun CZ, and Hotamisligil GS. Chemical chaperones reduce ER stress and restore glucose homeostasis in a mouse model of type 2 diabetes. *Science* 313: 1137–1140, 2006.
42. Patel JM and Block ER. Acrolein-induced injury to cultured pulmonary artery endothelial cells. *Toxicol Appl Pharmacol* 122: 46–53, 1993.
43. Petersen AMW, Magkos F, Atherton P, Selby A, Smith K, Rennie MJ, Pedersen BK, and Mittendorfer B. Smoking impairs muscle protein synthesis and increases the expression of myostatin and MAFbx in muscle. *Am J Physiol Endocrinol Metab* 293: E843–E848, 2007.
44. Pons M and Marin-Castano ME. Cigarette smoke-related hydroquinone dysregulates MCP-1, VEGF and PEDF expression in retinal pigment epithelium *in vitro* and *in vivo*. *PLoS One* 6: e16722, 2011.
45. Ramkumar HL, Zhang J, and Chan CC. Retinal ultrastructure of murine models of dry age-related macular degeneration (AMD). *Prog Retin Eye Res* 29: 169–190, 2010.
46. Rao RV, Castro-Obregon S, Frankowski H, Schuler M, Stoka V, del Rio G, Bredesen DE, and Ellerby HM. Coupling endoplasmic reticulum stress to the cell death program. An Apaf-1-independent intrinsic pathway. *J Biol Chem* 277: 21836–21842, 2002.
47. Romero-Ramirez L, Cao H, Nelson D, Hammond E, Lee AH, Yoshida H, Mori K, Glimcher LH, Denko NC, Giaccia AJ,

et al. XBP1 is essential for survival under hypoxic conditions and is required for tumor growth. *Cancer Res* 64: 5943–5947, 2004.
48. Song B, Scheuner D, Ron D, Pennathur S, and Kaufman RJ. Chop deletion reduces oxidative stress, improves beta cell function, and promotes cell survival in multiple mouse models of diabetes. *J Clin Invest* 118():: 3378–3389, 2008.
49. Tamaki N, Hatano E, Taura K, Tada M, Kodama Y, Nitta T, Iwaisako K, Seo S, Nakajima A, Ikai I, *et al.* CHOP deficiency attenuates cholestasis-induced liver fibrosis by reduction of hepatocyte injury. *Am J Physiol Gastrointest Liver Physiol* 294: G498–G505, 2008.
50. Tanriverdi H, Evrengul H, Kuru O, Tanriverdi S, Seleci D, Enli Y, Kaftan HA, and Kilic M. Cigarette smoking induced oxidative stress may impair endothelial function and coronary blood flow in angiographically normal coronary arteries. *Circ J* 70: 593–599, 2006.
51. Thornton J, Edwards R, Mitchell P, Harrison RA, Buchan I, and Kelly SP. Smoking and age-related macular degeneration: a review of association. *Eye (Lond)* 19: 935–944, 2005.
52. Tirosh B, Iwakoshi NN, Glimcher LH, and Ploegh HL. Rapid turnover of unspliced Xbp-1 as a factor that modulates the unfolded protein response. *J Biol Chem* 281: 5852–5860, 2006.
53. Wang AL, Lukas TJ, Yuan M, Du N, Handa JT, and Neufeld AH. Changes in retinal pigment epithelium related to cigarette smoke: possible relevance to smoking as a risk factor for age-related macular degeneration. *PLoS One* 4: e5304, 2009.
54. Welch WJ and Brown CR. Influence of molecular and chemical chaperones on protein folding. *Cell Stress Chaperones* 1: 109–115, 1996.
55. Xie Q, Khaoustov VI, Chung CC, Sohn J, Krishnan B, Lewis DE, and Yoffe B. Effect of tauroursodeoxycholic acid on endoplasmic reticulum stress-induced caspase-12 activation. *Hepatology* 36: 592–601, 2002.
56. Xu C, Bailly-Maitre B, and Reed JC. Endoplasmic reticulum stress: cell life and death decisions. *J Clin Invest* 115: 2656–2664, 2005.
57. Yu AL, Birke K, Burger J, and Welge-Lussen U. Biological effects of cigarette smoke in cultured human retinal pigment epithelial cells. *PLoS One* 7: e48501, 2012.
58. Zeng L, Zampetaki A, Margariti A, Pepe AE, Alam S, Martin D, Xiao Q, Wang W, Jin Z-G, Cockerill G, *et al.* Sustained activation of XBP1 splicing leads to endothelial apoptosis and atherosclerosis development in response to disturbed flow. *Proc Nat Acad Sci U S A* 106: 8326–8331, 2009.
59. Zhong Y, Li J, Wang JJ, Chen C, Tran J-TA, Saadi A, Yu Q, Le Y-z, Mandal MNA, Anderson RE, *et al.* X-Box Binding protein 1 is essential for the anti-oxidant defense and cell survival in the retinal pigment epithelium. *PLoS One* 7: e38616, 2012.

Address correspondence to:
Dr. Sarah X. Zhang
Departments of Ophthalmology and Biochemistry
Ira G Ross Eye Institute
University at Buffalo
SUNY Eye Institute
The State University of New York
Farber Hall 308
Buffalo, NY 14214

E-mail: xzhang38@buffalo.edu

Date of first submission to ARS Central, February 5, 2013; date of final revised submission, September 10, 2013; date of acceptance, September 22, 2013.

Abbreviations Used

AMD = age-related macular degeneration
ATF4 = activating transcription factor 4
CHOP = C/EBP homologous protein
CS = cigarette smoke
eIF2α = eukaryotic translation initiation factor 2α
ER = endoplasmic reticulum
GRP78 = glucose-regulated protein
HQ = hydroquinone
IRE1α = inositol-requiring enzyme 1α
IS/OS = inner segment/outer segment
ONL = outer nuclear layer
PBA = 4-phenyl butyric acid
PERK = PKR-like ER kinase
RPE = retinal pigment epithelium
TdT = terminal deoxynucleotidyl transferase
TUDCA = tauroursodeoxycholate
TUNEL = terminal deoxynucleotidyl transferase dUTP nick end labeling
UPR = unfolded protein response
XBP1 = X-box binding protein 1